DAPNIA/SPhN 95 11 03/1995

^{3}He Induced Reactions on ^{nat}Ag and ^{197}Au at 1.8, 3.6 and 4.8 GeV

J. Brzychczyk[1,3], E.C. Pollacco[1], C. Volant[1], R. Legrain[1], K. Kwiatkowski[2], K.B. Morley[2], E. Renshaw-Foxford[2], D.S. Bracken[2], V.E. Viola[2], N.R. Yoder[2], W.A. Friedman[4], R.G. Korteling[5], H. Breuer[6] and J. Cugnon[7].

DAPNIA

Le DAPNIA (Département d'Astrophysique, de physique des Particules, de physique Nucléaire et de l'Instrumentation Associée) regroupe les activités du Service d'Astrophysique (SAp), du Département de Physique des Particules Elémentaires (DPhPE) et du Département de Physique Nucléaire (DPhN).

Adresse : DAPNIA, Bâtiment 141
CEA Saclay
F - 91191 Gif-sur-Yvette Cedex

Communication présentée au :
XXXIII Winter Meeting on Nuclear Physics,
BORMIO, Italie
du 23 au 28 janvier 1995

^{3}He Induced Reactions on ^{nat}Ag and ^{197}Au at 1.8, 3.6 and 4.8 GeV

J. Brzychczyk[1,3], E.C. Pollacco[1], C. Volant[1], R. Legrain[1], K. Kwiatkowski[2], K.B. Morley[2], E. Renshaw-Foxford[2], D.S. Bracken[2], V.E. Viola[2], N.R. Yoder[2], W.A. Friedman[4], R.G. Korteling[5], H. Breuer[6] and J. Cugnon[7].

(1) CEA, DAPNIA/SPhN, CE Saclay, F-91191 Gif-sur-Yvette Cedex, France
(2) Dept. of Chemistry and IUCF, Indiana University, Bloomington, IN 47405, US
(3) Institut of Physics, Jagiellonian University, 30-059 Krakow, Poland
(4) Dept. of Physics, University of Wisconsin, Madison, WI 53706, US
(5) Dept. of Chemistry, Simon Fraser University, Burnaby, BC, Canada
(6) Dept. of Physics, University of Maryland, College Park, MD 20742, US
(7) Physique Nucléaire Théorique, Université de Liège, B-4000 Liège 1, Belgium

Abstract

The ^{3}He induced reactions on Ag and Au are studied using a large solid angle and low energy threshold detector array. The data show consistency with intranuclear cascade and expanding emitting source description. Charge moment analysis is presented.

When an energetic light ion of a few GeV interacts strongly with a nucleus we know that a significantly large portion of the incident kinetic energy is transferred to the target. Although it is interesting to study the processes which lead to high excitations our attention, as many presents at Bormio, is focused towards the study of the exit channel. Namely, we are trying to establish the physics that governs the decay of very hot nuclei. Of course multifragmentation is a word that sums this area of nuclear physics.

The interest behind light ions lies in the fact that they do not bring in large amounts of angular momentum into the system and little or no

compression. Of course, we are interested in compressing the nucleus and this we do with heavy ions, however the problem is that at the present it is difficult to unfold the effects which arise from compression to the ones that are brought about by thermal or other phenomena. This is where light ions become interesting. It is also important to add that with relatively small amounts of angular momentum and compression the prepared nucleus is less susceptible to have strong volume distortion, does making it less difficult to treat theoretically. For the experimentalist, we have to deal with small cross-sections and with difficulties related to beams at high velocities. However, this is in part recompensed by a simpler analysis; no projectile source and low kinematic distortion.

The experiment was performed at the Laboratoire National Saturne at Saclay using a set-up essentially consisting of three pieces of equipment. At forward angles we detected the quasi-projectile fragments in a plastic wall ARCOLE [1] which covered angles approximately between 1.5° to 10° with respect to the beam direction. Also at forward angles, 5° to 10°, we detected heavy fragments in bare Si with velocity thresholds down to 0.15 cm/ns.

The angular range of 14° to 166° was covered using the detector ISiS [2]. This consists of 162 ion chamber (17 torr C_3F_8, 30 mm deep) - Si (500 μm) - CsI (28 mm) telescopes. The geometrical coverage of ISiS was ~70% of 4π. This arrangement allows a low energy threshold and good charge separation for Z=1 up to 16. Isotope separation is obtained for those particles which stop in the CsI. The detectors were energy calibrated and all IC-Si and Si-CsI spectra were overlaid thus allowing a common set of windows. This analysis gives a dynamic range of 1-25 A· MeV. Beam halo related events were removed via an active collimator placed upstream. Details of the beam intensities, targets, electronics, active collimator and other details are given elsewhere [3]. The detection trigger for the whole of the system was set to multiplicity two or greater for particles hitting the Si(ISiS) counters.

The systems studied are ^{3}He (1.8, 3.6, 4.8 GeV) + ^{nat}Ag and ^{3}He (1.8, 4.8 GeV) + ^{197}Au. In this contribution we show data coming only from ISiS. The objective here is to give a rough overview of the data followed by principal results obtained so far. At the end of this contribution we include a preliminary charge moment analysis.

In fig.1 the light charged particles, N_{LCP}, intermediate mass fragments (IMF $3 \leq Z \leq 20$), N_{IMF}, and total multiplicity distributions are given. No detector filter correction is applied. For both targets and all incident energies (not shown) the IMF contribution is relatively small. Comparison of the two targets shows that the IMF and LCP multiplicities arising from Au extend to higher values then for Ag with the same bombarding energy.

Before presenting the next two results it is important to stress that even for the present wide geometrical coverage the experimental filter plays a role. Also, in plotting different parameters one is susceptible to obtain evident and sometime less evident auto-correlations. The correlation between N_{IMF} and N_{LCP} for ^{197}Au is given in fig.2. We make three comments. (1) The no IMF contribution is significant and the distribution extends to high N_{LCP} values. This shows that these events have a relatively high cross section and that they play an important role in the exit channel. (2) The N_{LCP} distributions as a function of N_{IMF} have maxima located at N_{LCP} = 8-10. (3) The widths are relatively large. With regards to this last comment we have used an evaporation code [4] and the WIX event generator [5] and filtered the output by the detector acceptance. From this analysis we conclude that the observed widths are not enhanced by more than 30%. Figure 3 is a plot of N_{IMF} as a function of the total observed kinetic energy. The auto-correlation is evident, however the data does show the calorimetric range with increasing N_{IMF}. Now, taking the mean value of N_{IMF} and plotting it as a function of N_{LCP} or total multiplicity, N_{tot}, or total observed charge, Z_{obs}, gives fig.4. The variable E_{th} = ΣE_i, where (E_i) are the kinetic energies for the detected particles with $E_i \leq 25$ Z·MeV. The construction of E_{th} allows the removal of those LCP which have a preequilibrium character and should therefore relate to the energy liberated in the cooling processes. Thus from fig.4 we conclude that $<N_{IMF}>$ and Z_{obs} are correlated to the energy deposition.

The top panel of fig.5 shows the N_{IMF} distribution for ^{nat}Ag at three E_{beam}. The multiplicity increases in going from 1.8 to 3.6 GeV, however we observe no or even a small decrease in reaching 4.8 GeV from 3.6 GeV. Plotting the $N_i/\Sigma N_i$ as a function of E_{th} or Z_{obs} (with the 25 Z·MeV condition) for the three incident energies show results which are consistent with those of fig. 5a. Namely, a lack of yield

at 1.8 GeV with respect to 3.6 GeV and the 3.6 GeV and 4.8 GeV data having very similar distributions. These results suggest that the energy deposition by ^{3}He on ^{nat}Ag saturates about 3.6 GeV. For the gold target because of the limited beam energy range investigated, no such conclusion can be drawn.

In order to investigate this saturation effect we have performed calculations with the INC code [6] which, in the version used, contains the nucleons in a potential. To extract the excitation energy the calculation was stopped at 30 fm/c at which point the nucleons start to have thermal energies and to be emitted isotropically. The calculated excitation energy, E^{*}, distributions are given in the lower panel of fig.5 and show trends with E_{beam} similar to the data. Namely, we find only minor changes in E^{*} distribution between 3.6 and 4.8 GeV. The INC code ISABEL [7] shows similar trends [3]. Thus, we conclude that the INC calculation gives a reasonable description of the energy deposition.

Sample energy spectra at $\Theta = 43^{\circ}$ and 119° for carbon fragments in the reaction ^{3}He + ^{197}Au at 4.8 GeV are given in fig.6. For both pannels, the spectra are given with windows on Z_{obs}= 1-10, Z_{obs}= 11-20, Z_{obs}= 51-60 and shown in that order starting from the top. Two remarks can be made. (1) With angle the spectra retain the same general shape with a relatively small contraction in energy for the larger angle. This is characteristic of a source moving in the forward direction. In fact, contour plots of invariant cross section show a unique source with a small velocity of approximately 0.015 c [3,8]. (2) Of interest is that with increasing Z_{obs} the spectra are modified whereby the Coulomb peak is flattened with an enhanced yield at lower energy. Excluding effects like sequential binary decay, the data suggest that at high energy transfer the IMF have a source within a diluted nucleon volume where the Coulomb potential becomes strongly attenuated.

The IMF observed multiplicities for ^{nat}Ag (circles) and ^{197}Au (squares) for the data set at 4.8 GeV are given in fig.7. Correcting for the angular distribution as well as the geometrical efficiency of ISiS gives mean multiplicities of $<N_{IMF}(Ag)>$= 1.4 and $<N_{IMF}(Au)>$= 2.0. These results are obtained when imposing that at least one IMF is produced in reconstucted events [3,8]. Values from heavy ion induced reactions with similar total composite system give values which are

not significantly higher (see E. De Fillipo et al. at this conference). However the value ($<N_{IMF}(Au)>= 3.8$) obtained by Lips et al. [9] for ^{4}He(4 GeV) + ^{197}Au is rather larger than the one extracted in the present analysis.

From the INC calculation we show that after the emission of the pre-equilibrium particles, the residual nucleus is left with E^* which extends to values as large as 10-15 A·MeV. To confront our data with a model description we have coupled the expanding emitting source (EES) model [10] with the INC calculations [11]. The EES model assumes statistical emission of fragments and treats expansion in terms of a giant monopole oscillation driven by thermal pressure. The binding energy of the instantaneous source follows a parabolic density dependence, governed by an effective compressibility parameter K. In these calculations, K = 144 was employed. In this model, IMF emission occurs sequentially, but on a fast time scale ($\leq$ 70 fm/c), during the expansion. If the thermal pressure is sufficient to reach nuclear densities of $\rho/\rho_o \simeq 0.3$, instantaneous multifragmentation of the residue then occurs. At this point, surface fragment emission is replaced by volume emission in calculating the fragment spectra. Volume emission may also be interpreted in terms of simultaneous breakup of the expanded residue.

The calculated results have been filtered through the ISiS detector geometry for comparison with the measured IMF multiplicity distributions for the 4.8 GeV ^{3}He + ^{197}Au,^{nat}Ag reactions as shown in fig.7. For ^{197}Au the calculation describes the data well for most of the IMF cross section. For ^{nat}Ag, the agreement is somewhat poorer, but may be improved by more exact treatment of detector thresholds in the simulation. In comparing the INC/EES model with the data for these two dissimilar targets, no attempt has been made to adjust the input parameters, which are identical for both targets and based on Ref. [11]. Overall, the calculations and data are consistent only if expansion is included in the model.

Prediction of the spectral shapes by the INC/EES model are compared with the data in fig.6. The trends parallel one another well; i.e. the Coulomb peaks broaden and shift downward in energy, while the spectral tails harden with increasing Z_{obs}. Particular success is achieved in reproducing the data for large Z_{obs} values, where the model should be most appropriate for comparison with the data. In terms of the model, the overall behavior can be explained as follows. The most energetic fragments are emitted early in the expansion from a

high Z source near normal matter density; they also receive a boost in energy from the source expansion velocity. Since both the excitation energy and expansion velocity should scale with Z_{obs}, the spectral slopes are expected to become systematically flatter with increasing Z_{obs}. For systems that expand to the critical breakup density ($\rho/\rho_o \sim 0.3$), the expansion velocity is near zero and the system is highly distended. Thus, fragments emitted at this stage experience greatly reduced Coulomb repulsion, which is rather influenced by effects of volume emission with a random distribution of fragment velocities. Thus, very low energy fragments with a broad energy distribution result.

Different fragmentation models could be verified by studying moments of the fragments size distributions and their fluctuations [12–18]. In our preliminary work we have examined correlations between the reduced charge moments S_3 and S_2, and distributions of the reduced variance, γ_2 [12–14].

For both systems ^{3}He (4.8 GeV) + ^{197}Au,^{nat}Ag strong linear correlations are observed when $\ln S_3$ is plotted against $\ln S_2$, and give the same slope parameter, τ of 2.2 ± 0.08. Similar values are found in other gold fragmentation data, in agreement with percolation and liquid-gas predictions [12,18]. However, τ is not very sensitive to the model [17].

A more sensitive observable to the details of the fragment size distribution is the reduced variance, γ_2 [13,14]. Fig.8 shows the average γ_2 of events with a given multiplicity for the ^{3}He (4.8 GeV) + ^{197}Au data. The first plot is for all detected events. However, it is important to note that, as predicted by the INC code, we expect that in this distribution the dominant contribution comes from low excitation energy events. Such events consist of several LCP plus one heavy residue or two fission fragments. Because heavy fragments are not detected in ISiS and observed fission fragments are excluded in our analysis, the average γ_2 is small, at least for the low multiplicity range. Further, it has to be recalled that the distribution could be modified by the detector filter.

The total charge of the fragmenting system is not well defined because of the entrance channel employed to raise the system to a fragmentation condition. For example, the INC calculations predict an average charge of 71 with rms of 3.2 for nuclei excited above 4 A·MeV in the ^{3}He (4.8 GeV) + ^{197}Au reaction. In our analysis, to approach

the "complete events" we have placed Z_{obs} windows of $Z_{obs} \geq 50$, 55 and 60 as shown in fig.8. These conditions ensure that a large portion of the total charge is detected and that evaporation/fission events are rejected.

As can be seen in fig.8 the shape of the distribution does not change with increasing threshold Z_{obs}. $<\gamma_2>$ is peaked at multiplicity 11 and reaches value of 2.3. These values can be compared with those predicted by different fragmentation models [14,16] and other gold data [13]. Distribution of $<\gamma_2>$ is usually plotted against the reduced multiplicity defined as the ratio of a given to the maximum multiplicity [13,14]. To a first approximation, taking the size of the fragmenting system of 71 charge units (as predicted by INC) we get the position of the maximum at a reduced multiplicity about 0.15. This is less than the percolation value, 0.25, and seems to be in a better agreement with the statistical model of Gross [16]. It should be stressed that the data, gated even by large value of Z_{tot} may still be influenced by the detector acceptance. A strict comparison is to sieve the calculated events through the experimental filter.

To examine the effect of excluding a larger portion of the preequilibrium particles we have redone the analysis using a upper energy threshold of 18 A·MeV. The $<\gamma_2>$ distributions change very little, shifting down by about 0.05 for all Z_{tot} gates. This is in agreement with conclusion that the critical exponents are unaffected by the inclusion of cascade protons [18].

To summarize, in this contribution we have concentrated in showing the data from the reaction ^{3}He (1.8, 3.6, 4.8 GeV) + ^{nat}Ag, ^{197}Au using a large solid angle and low energy threshold detector array. A salient result is the saturation of deposit energy of ^{3}He + Ag at 3.6 GeV which is consistent with INC codes. INC calculation followed by EES does describe the IMF and IMF spectra which suggests that for the higher energy deposit the nucleus expands under the thermal pressure leading to a breakup of the nucleus into fragments. Charge moment analysis looks promising and en extensive study is underway.

REFERENCES

[1] Y. Terrien et al., Phys. Lett. B294 (1992) 40.

[2] K. Kwiatkowski et al., Nucl. Instr. Meth. A353 (1994) 212.

[3] K.B. Morley, Ph.D. thesis, Indiana University, 1994; Indiana Nuclear Chemistry Report INC-40007-102.

[4] D. Durand, private communication.

[5] J. Randrup, Comput. Phys. Commun. 77 (1993) 153.

[6] J. Cugnon et al., Nucl. Phys. A379 (1982) 555; A462 (1987) 751.

[7] Y. Yariv and Z. Fraenkel, Phys. Rev. C24 (1981) 488.

[8] K. Kwiatkowski et al., accepted for publication in Phys. Rev. Lett.

[9] V. Lips et al., Phys. Rev. Lett. 72 (1994) 604.

[10] W.A. Friedman, Phys. Rev. C42 (1990) 667.

[11] K. Kwiatkowski et al., Phys. Rev. C49 (1994) 1516.

[12] X. Campi, J. Phys. A19 (1986) L917.

[13] X. Campi, Phys. Lett. B208 (1988) 351.

[14] X. Campi, H. Krivine, Z. Phys. A344 (1992) 81.

[15] H.R. Jaqaman, D.H.E. Gross, Nucl. Phys. A524 (1991) 321.

[16] D.H.E. Gross, Rep. Prog. Phys. 53 (1990) 605.

[17] J. Richert and P. Wagner, Nucl. Phys. A517 (1990) 399.

[18] M.L. Gilkes et al., Phys. Rev. Lett. 73 (1994) 1590.

FIGURES

FIG. 1. Observed IMF, LCP, and total charged particle multiplicity distributions for the ^{3}He (4.8 GeV) + ^{nat}Ag (top), ^{197}Au (bottom) reactions.

FIG. 2. Observed IMF versus LCP multiplicity distribution for the ^{3}He (4.8 GeV) + ^{197}Au reaction.

FIG. 3. Observed IMF multiplicity as a function of observed total kinetic energy for the ^{3}He (4.8 GeV) + ^{197}Au.

FIG. 4. Average IMF multiplicity, $<N_{IMF}>$, as a function of light charged particle multiplicity, N_{LCP} (top-left); total charged particle multiplicity, N_{tot} (top-right); total observed charge, Z_{obs} (bottom-left) and total thermal energy, E_{th} (bottom-right).

FIG. 5. Observed IMF multiplicity distributions (a) and INC model prediction for excitation energy distributions (b) in the ^{3}He (1.8, 3.6, 4.8 GeV) + ^{nat}Ag reactions.

FIG. 6. Laboratory energy spectra for carbon fragments in the ^{3}He (4.8 GeV) + ^{197}Au reactions, gated on total observed charge. Points are data and lines are predictions of the INC/EES model (see text). Calculations are normalized to the data so that maximum probabilities are equal in magnitude.

FIG. 7. Observed IMF multiplicity distributions for the ^{3}He (4.8 GeV) + ^{nat}Ag, ^{197}Au reactions. Points are data. Histograms show predictions of the INC/EES model corrected for the detector geometry.

FIG. 8. Average reduced variance, $<\gamma_2>$, as a function of total observed charged particle multiplicity for ^{3}He (4.8 GeV) + ^{197}Au reactions, gated on total observed charge.

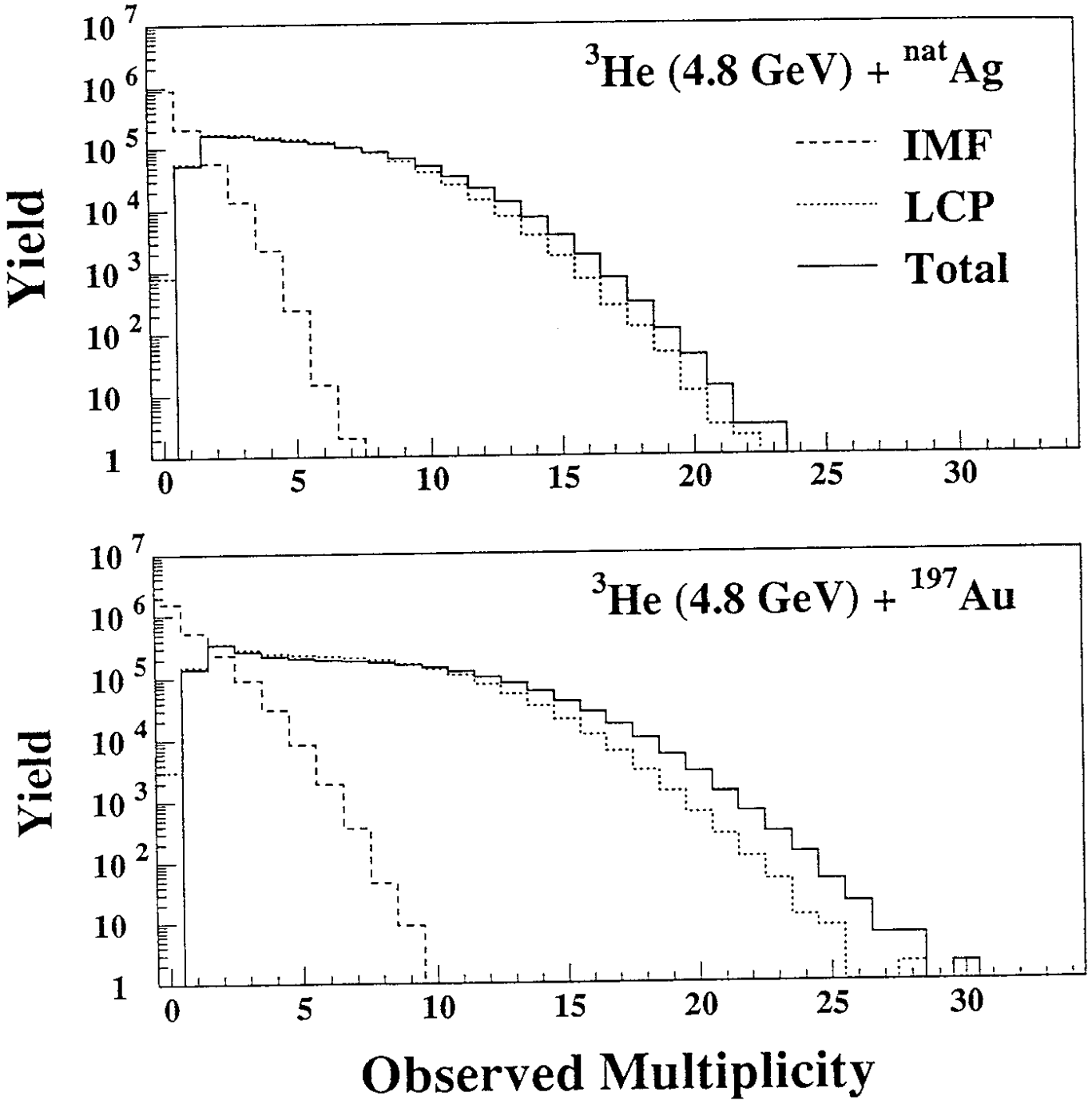
^{3}He (4.8 GeV) + ^{nat}Ag
IMF
LCP
Total
^{3}He (4.8 GeV) + ^{197}Au
Yield
Yield
Observed Multiplicity

Fig. 1

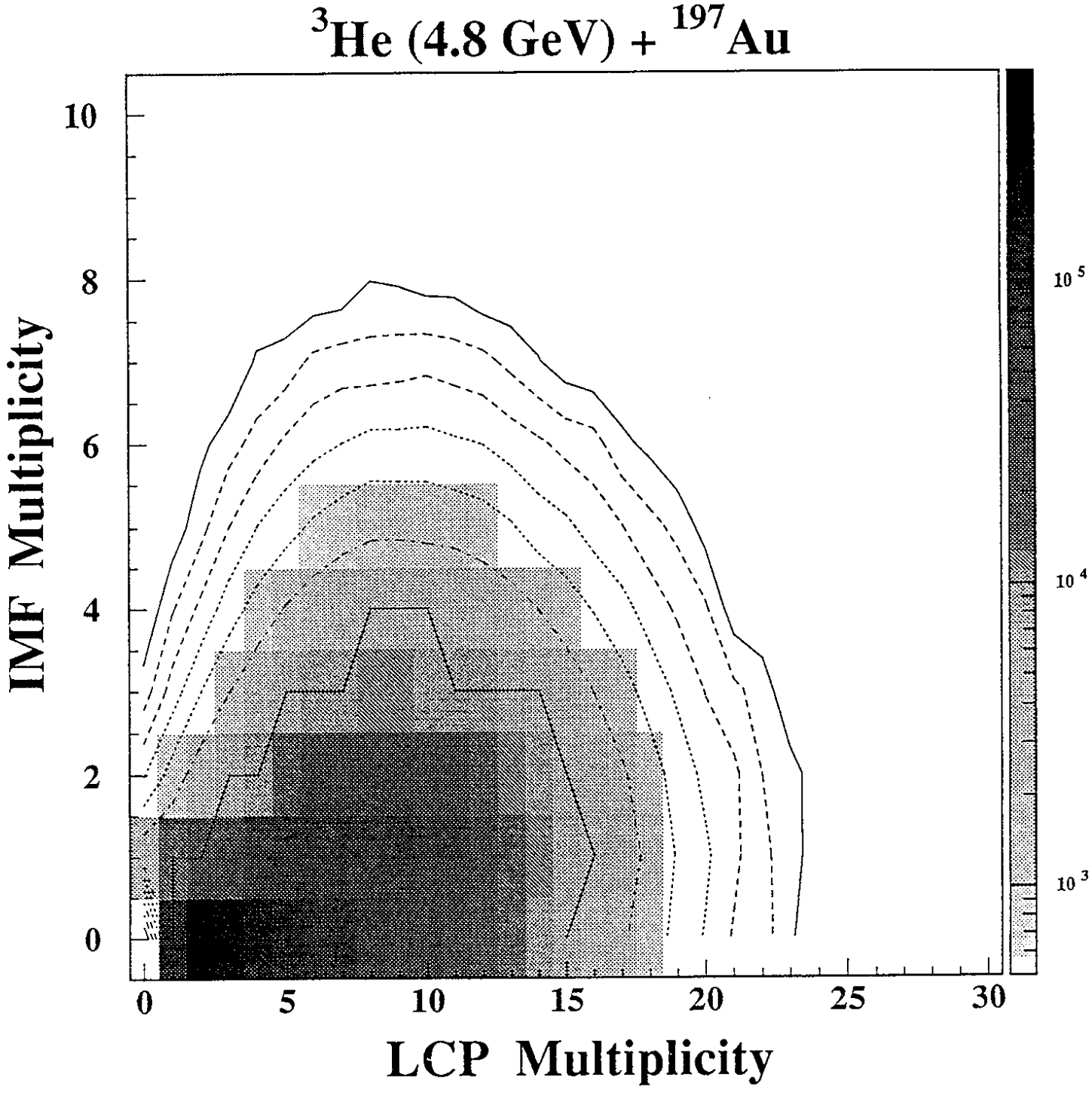
^{3}He (4.8 GeV) + ^{197}Au
IMF Multiplicity
LCP Multiplicity
0
2
4
6
8
10
0
5
10
15
20
25
30
10^{5}
10^{4}
10^{3}

Fig. 2

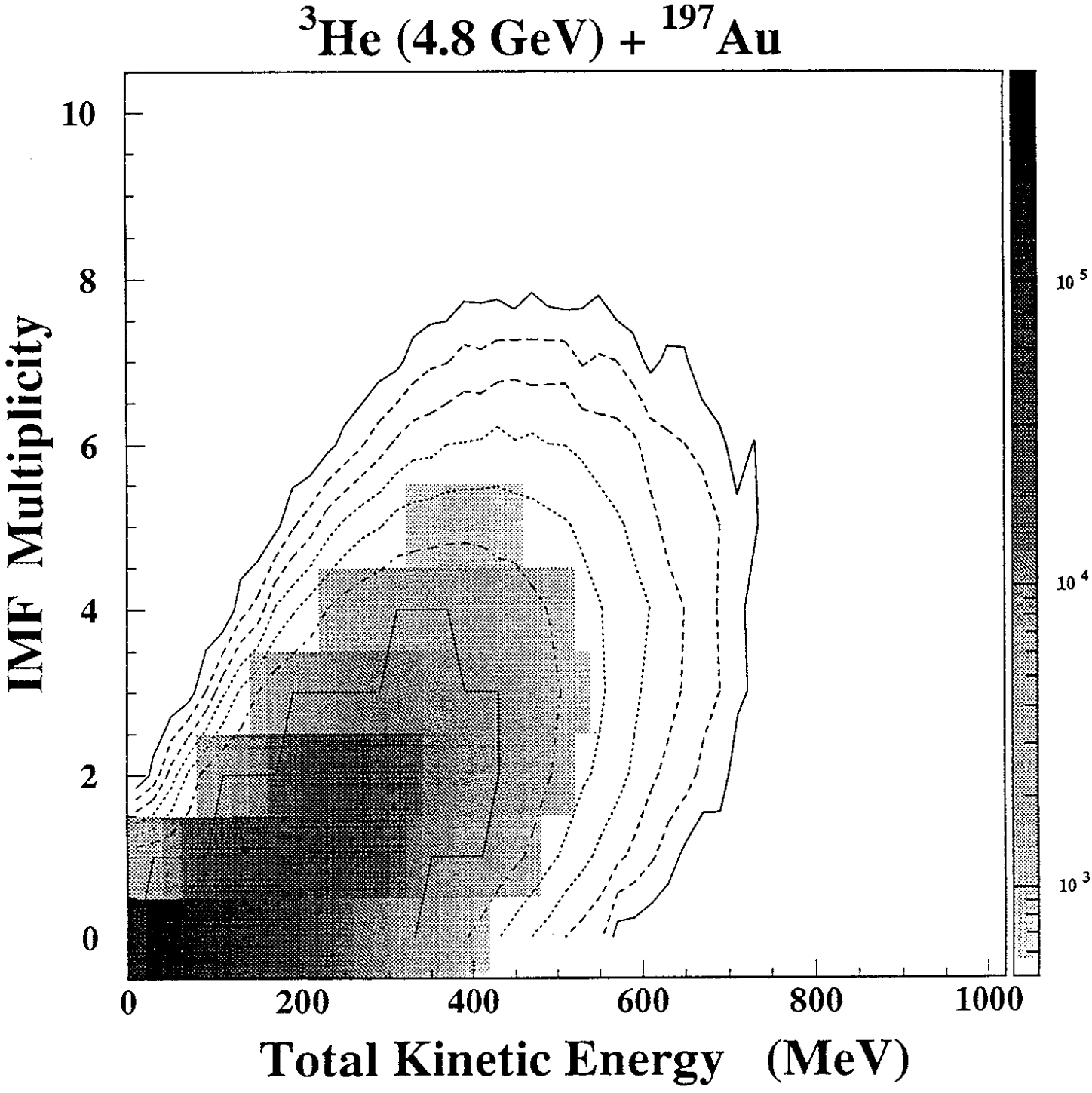
^{3}He (4.8 GeV) + ^{197}Au
IMF Multiplicity
0
2
4
6
8
10
0
200
400
600
800
1000
Total Kinetic Energy (MeV)
10^{5}
10^{4}
10^{3}

Fig. 3

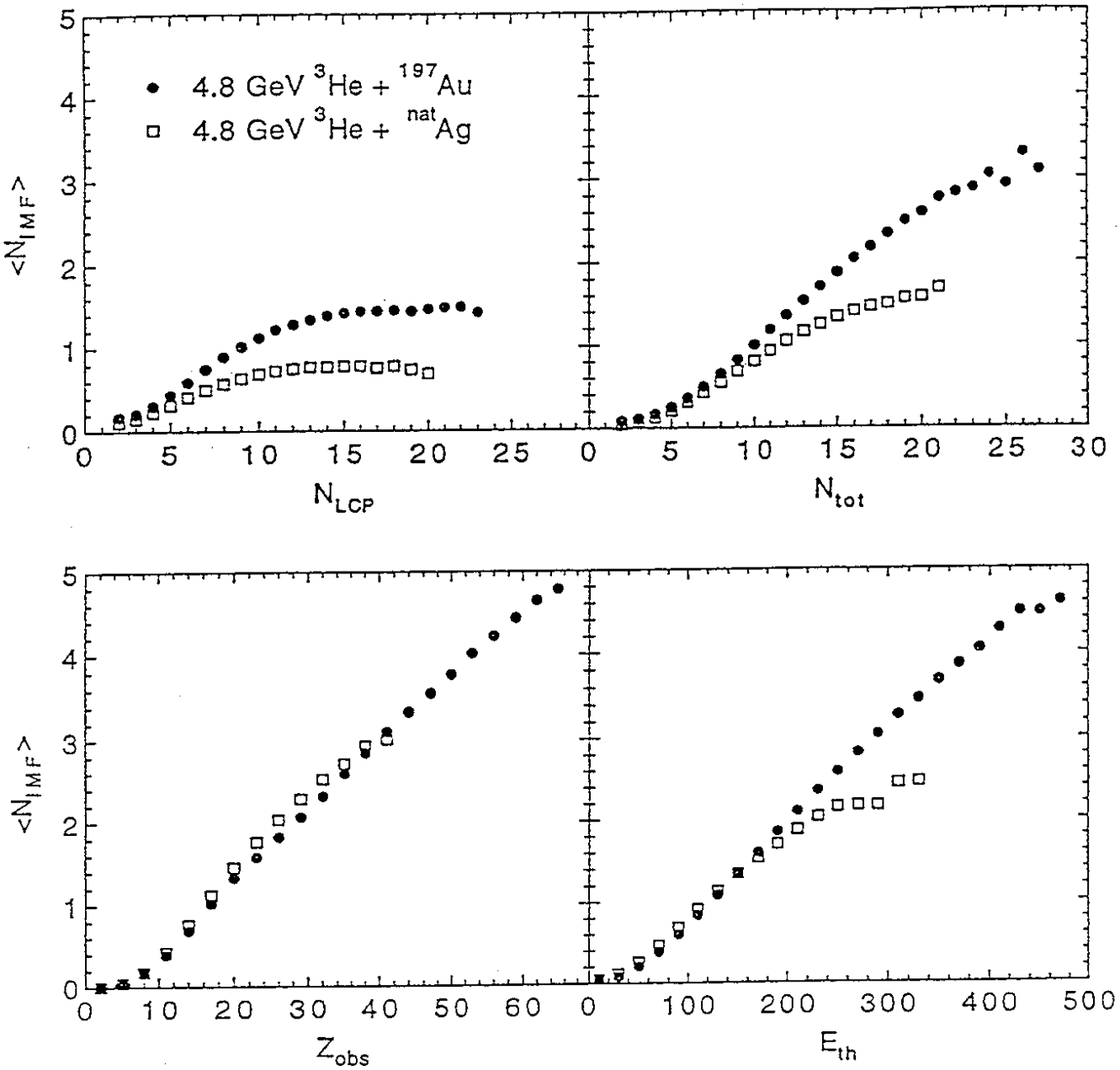

Fig. 4

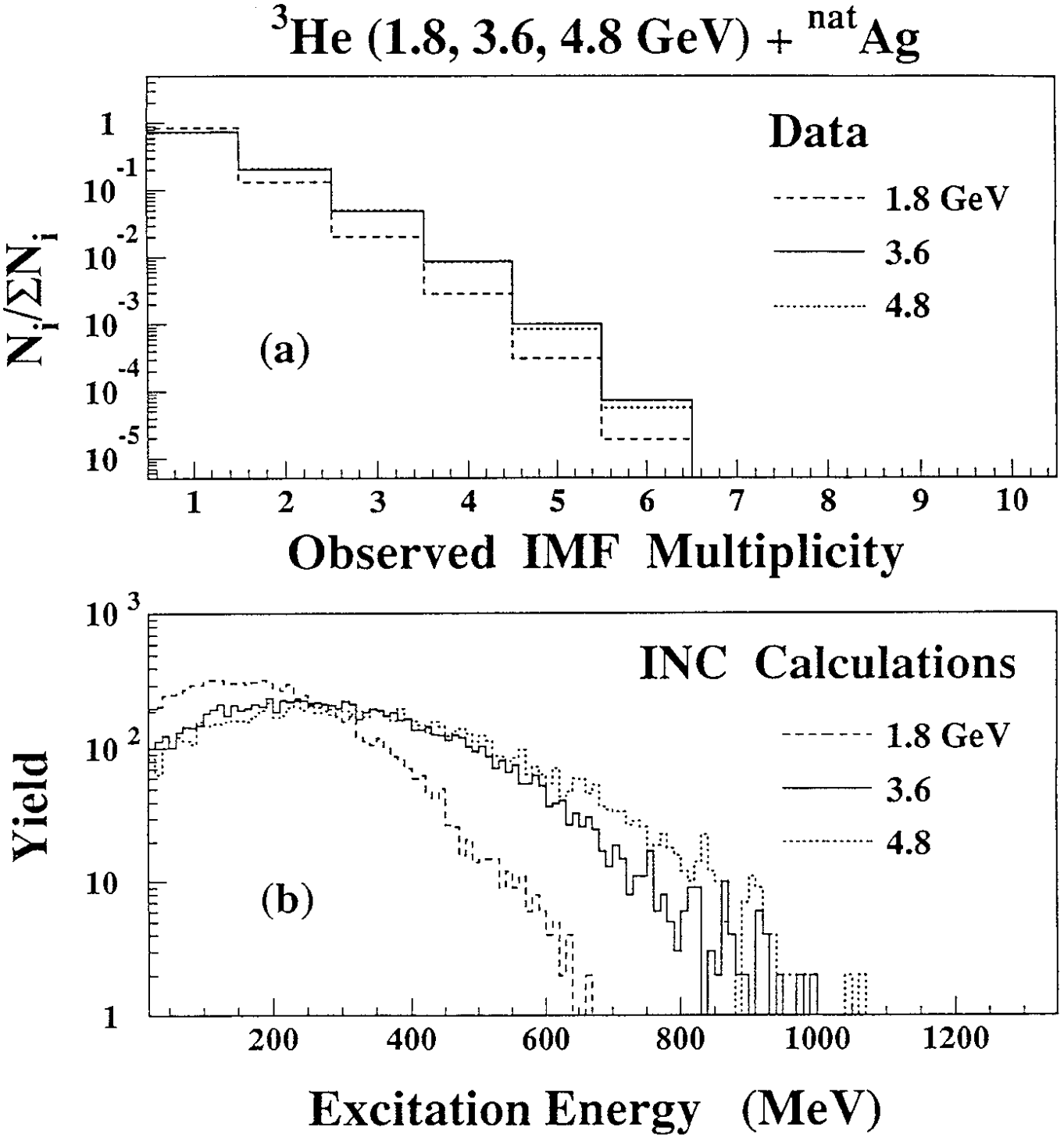
^{3}He (1.8, 3.6, 4.8 GeV) + ^{nat}Ag
Data
1.8 GeV
3.6
4.8
(a)
$N_i/\Sigma N_i$
Observed IMF Multiplicity
INC Calculations
1.8 GeV
3.6
4.8
(b)
Yield
Excitation Energy (MeV)

Fig. 5

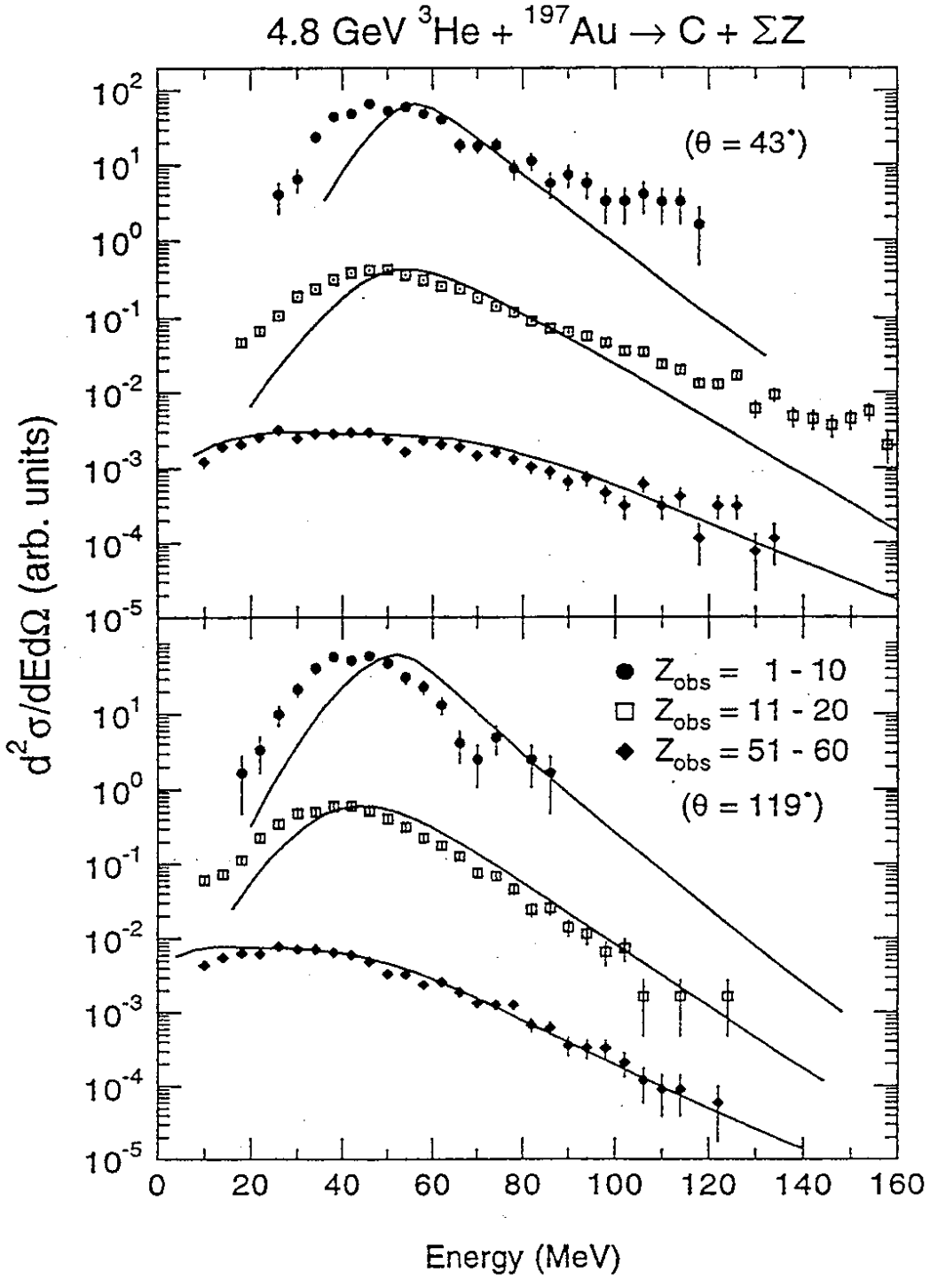
4.8 GeV ^{3}He + ^{197}Au → C + ΣZ
(θ = 43°)
(θ = 119°)
Z_{obs} = 1 - 10
Z_{obs} = 11 - 20
Z_{obs} = 51 - 60
$d^2\sigma/dEd\Omega$ (arb. units)
Energy (MeV)

Fig. 6

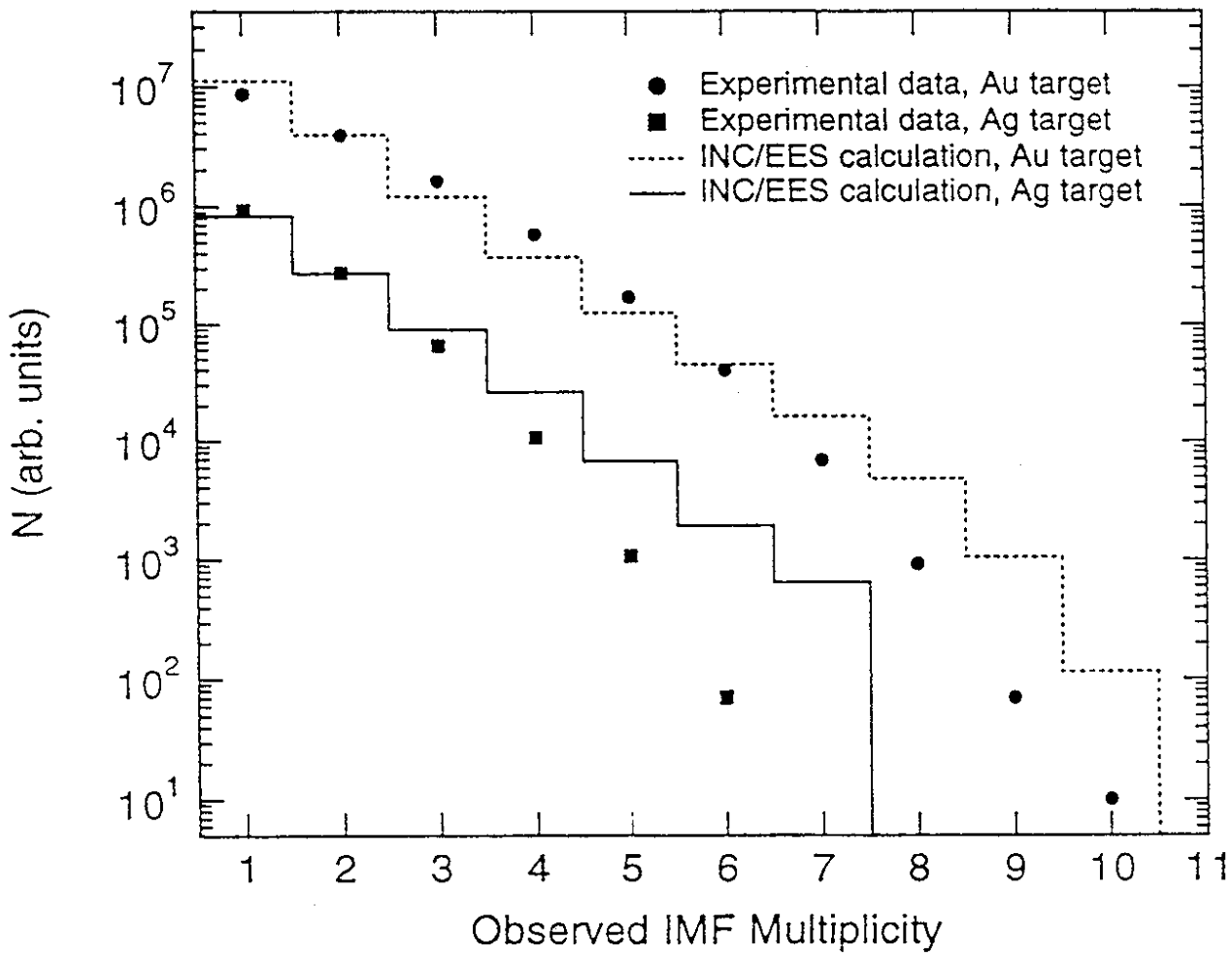
Experimental data, Au target
Experimental data, Ag target
INC/EES calculation, Au target
INC/EES calculation, Ag target
N (arb. units)
Observed IMF Multiplicity
10^7
10^6
10^5
10^4
10^3
10^2
10^1
1
2
3
4
5
6
7
8
9
10
11

Fig. 7

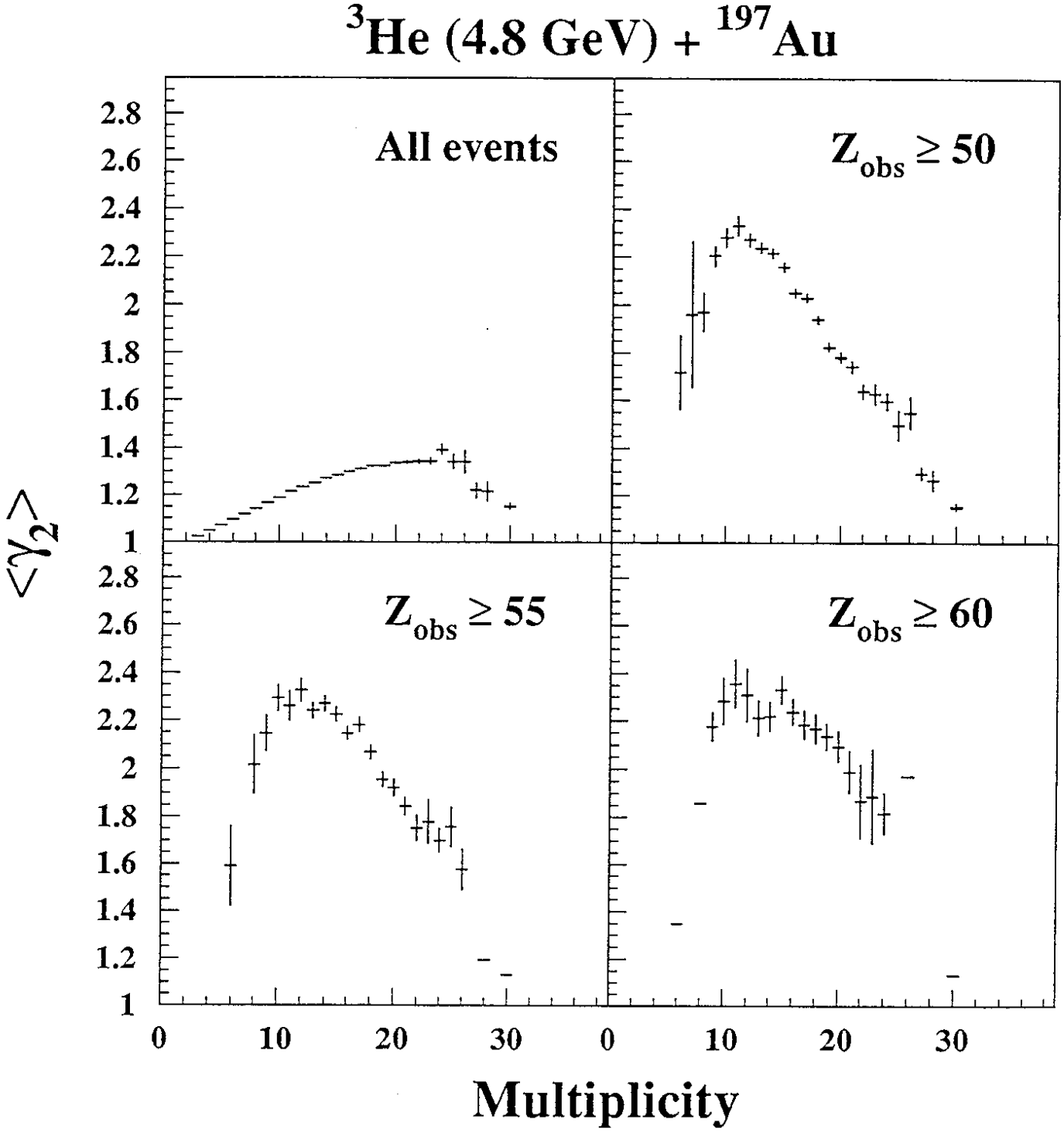
^{3}He (4.8 GeV) + ^{197}Au
All events
$Z_{obs} \geq 50$
$Z_{obs} \geq 55$
$Z_{obs} \geq 60$
$\langle \gamma_2 \rangle$
Multiplicity
2.8
2.6
2.4
2.2
2
1.8
1.6
1.4
1.2
1
0
10
20
30

Fig. 8